

Wedge-shaped HfO_2 buffer layer-induced field-free spin-orbit torque switching of HfO_2/Pt/Co structure

Jian-Hui Chen(陈建辉), Meng-Fan Liang(梁梦凡), Yan Song(宋衍), Jun-Jie Yuan(袁俊杰), Meng-Yang Zhang(张梦旸), Yong-Ming Luo(骆泳铭), and Ning-Ning Wang(王宁宁)

Citation: Chin. Phys. B, 2024, 33 (**4**): 047503. DOI: 10.1088/1674-1056/ad1a88
Journal homepage: http://cpb.iphy.ac.cn; http://iopscience.iop.org/cpb

What follows is a list of articles you may be interested in

Oscillation of Dzyaloshinskii-Moriya interaction driven by weak electric fields

Runze Chen(陈润泽), Anni Cao(曹安妮), Xinran Wang(王馨苒), Yang Liu(柳洋), Hongxin Yang(杨洪新), and Weisheng Zhao(赵巍胜)

Chin. Phys. B, 2024, 33 (**2**): 027501. DOI: 10.1088/1674-1056/ad0f85

Topological magnetotransport and electrical switching of sputtered antiferromagnetic $Ir_{20}Mn_{80}$

Danrong Xiong(熊丹荣), Yuhao Jiang(蒋宇昊), Daoqian Zhu(朱道乾), Ao Du(杜奥), Zongxia Guo(郭宗夏), Shiyang Lu(卢世阳), Chunxu Wang(王春旭), Qingtao Xia(夏清涛), Dapeng Zhu(朱大鹏), and Weisheng Zhao(赵巍胜)

Chin. Phys. B, 2023, 32 (**5**): 057501. DOI: 10.1088/1674-1056/acb9ec

Orbital torque of Cr-induced magnetization switching in perpendicularly magnetized Pt/Co/Pt/Cr heterostructures

Hongfei Xie(谢宏斐), Yuhan Chang(常宇晗), Xi Guo(郭玺), Jianrong Zhang(张健荣), Baoshan Cui(崔宝山), Yalu Zuo(左亚路), and Li Xi(席力)

Chin. Phys. B, 2023, 32 (**3**): 037502. DOI: 10.1088/1674-1056/aca6d7

Spin-orbit torque in perpendicularly magnetized [Pt/Ni] multilayers

Ying Cao(曹颖), Zhicheng Xie(谢志成), Zhiyuan Zhao(赵治源), Yumin Yang(杨雨民), Na Lei(雷娜), Bingfeng Miao(缪冰锋), and Dahai Wei(魏大海)

Chin. Phys. B, 2023, 32 (**10**): 107507. DOI: 10.1088/1674-1056/acee57

Skyrmion-based logic gates controlled by electric currents in synthetic antiferromagnet

Linlin Li(李林霖), Jia Luo(罗佳), Jing Xia(夏静), Yan Zhou(周艳), Xiaoxi Liu(刘小晰), and Guoping Zhao(赵国平)

Chin. Phys. B, 2023, 32 (**1**): 017506. DOI: 10.1088/1674-1056/ac9b01

Wedge-shaped HfO_2 buffer layer-induced field-free spin–orbit torque switching of HfO_2/Pt/Co structure

Jian-Hui Chen(陈建辉)[1], Meng-Fan Liang(梁梦凡)[1], Yan Song(宋衍)[1], Jun-Jie Yuan(袁俊杰)[1], Meng-Yang Zhang(张梦旸)[2], Yong-Ming Luo(骆泳铭)[1,†], and Ning-Ning Wang(王宁宁)[1]

[1] *School of Electronics and Information Engineering, Hangzhou Dianzi University, Hangzhou* 310018, *China*
[2] *Covestro (Shanghai) Investment Co., Ltd, Shanghai* 200126, *China*

(Received 25 September 2023; revised manuscript received 26 December 2023; accepted manuscript online 4 January 2024)

Field-free spin–orbit torque (SOT) switching of perpendicular magnetization is essential for future spintronic devices. This study demonstrates the field-free switching of perpendicular magnetization in an HfO_2/Pt/Co/TaO_x structure, which is facilitated by a wedge-shaped HfO_2 buffer layer. The field-free switching ratio varies with HfO_2 thickness, reaching optimal performance at 25 nm. This phenomenon is attributed to the lateral anisotropy gradient of the Co layer, which is induced by the wedge-shaped HfO_2 buffer layer. The thickness gradient of HfO_2 along the wedge creates a corresponding lateral anisotropy gradient in the Co layer, correlating with the switching ratio. These findings indicate that field-free SOT switching can be achieved through designing buffer layer, offering a novel approach to innovating spin–orbit device.

Keywords: spin–orbit torque, field-free switching, HfO_2 buffer layer

PACS: 75.70.Tj, 85.75.–d, 75.70.–i **DOI:** 10.1088/1674-1056/ad1a88

1. Introduction

Electrical manipulation of magnetization is pivotal for future ultralow-power, nonvolatile memory, and logic devices. Spin–orbit torque (SOT)-induced magnetization switching, facilitated by the spin Hall effect or Rashba–Edelstein effects, is a leading technique.[1,2] The SOT transforms charge current into spin current, which exerts a torque on the magnetization. The SOT demonstrates significant advantages over conventional spin transfer torque (STT)-based devices in terms of device longevity,[3] reduced power consumption,[4] and faster operation.[5] Generally, the polarization direction of the spin current induced by SHE or Rashba–Edelstein effects is in-plane, and it is symmetric with respect to the upward magnetization and downward magnetization. Therefore, to realize the deterministic switching, the symmetry of the system has to be broken, and an auxiliary in-plane magnetic field is needed.[6–8] The existence of the on-chip magnetic field sets a major obstacle to the full electrical control of the magnetization.[9] Recently, various methods have been proposed to realize field-free switching, such as designing a built-in effective field,[10–13] creating composition gradients in film structures, employing unconventional out-of-plane polarized spin currents,[9,14,15] or utilizing asymmetric structures such as U-shaped geometry[16] or wedge structures. Wedge-shaped ferromagnetic layers,[17] heavy metal spin source layers,[18] capping layers,[19] and NM insertion layers[20] have shown potential in facilitating field-free switching.

Additionally, recent reports suggest that insulator buffer layers can promote field-free switching in MgO/Pt/Co structures, thus attracting considerable attention.[21] The current understanding attributes this phenomenon to the spin reflection-induced out-of-plane polarized spin current.[21] However, the generation of novel out-of-plane spin currents by reflection of the conventional in-plane spin Hall effect remains an open question. Moreover, buffer layer-induced field-free switching has been observed mainly in MgO systems. Investigating the occurrence and characteristics of buffer layer-induced field-free switching in different materials, is essential for understanding the buffer layer-induced switching mechanism. The HfO_2, a promising high-K and ferroelectric material,[22] has been shown to change the interfacial electron structure and enhance interface SOT when used as a capping layer.[23] Exploring the influence of HfO_2 as a buffer layer on SOT is a critical area of research, however, it remains lacking.

In this study, the SOT switching of perpendicular magnetization is reported by using HfO_2 as the buffer layer in an HfO_2/Pt/Co/TaO_x structure. Field-free switching is achieved with a wedge-shaped HfO_2 layer, but not with a flat HfO_2 buffer layer. The field-free switching ratio is tunable by varying the HfO_2 thickness, with a maximum efficiency at 25 nm. This is linked to the lateral anisotropy gradient in the Co layer, caused by the wedge-shaped HfO_2 buffer layer. The study demonstrates that the anisotropy of the Co layer can be tuned by the HfO_2 buffer layer thickness, and the thickness gradient

[†]Corresponding author. E-mail: ymluo@hdu.edu.cn

© 2024 Chinese Physical Society and IOP Publishing Ltd

of HfO_2 along the wedge structure leads to a lateral anisotropy gradient in the Co layer. The anisotropy is most sensitive to thickness variation at 25 nm for HfO_2, aligning with the optimized switching ratio. Additionally, the spin–orbit efficiency can be adjusted by the HfO_2 layer. These results demonstrate that the field-free SOT switching can be achieved by designing a buffer layer, which presents a new method of designing spin–orbit devices.

2. Sample preparation and film characterization

In this study, HfO_2/Pt/Co/TaO_x multilayers were deposited on Si/SiO_2 substrates by using high-vacuum magnetron sputtering. The structure is schematically shown in Fig. 1(a).

To study the influence of the HfO_2 buffer layer on the SOT-induced magnetization switching, we only changed the the thickeness of the buffer layer, while the thicknesses of other films were fixed, with Pt(3)/Co(1.4)/TaO_x(2) (number in parentheses is in nanometers). The HfO_2 buffer layer was deposited at room temperature. We both fabricated the films with wedge-shaped and uniform HfO_2. The HfO_2 was wedge-shaped unless otherwise stated. To form a wedge-shaped HfO_2, an oblique angle sputtering technique was used, where the substrate was not rotated and was maintained at a fixed angle relative to the HfO_2 target.[24] By controlling the oblique direction of the target with respect to the substrate, the wedge directions could be controlled (fixed along the y axis in this study) as shown in Fig. 1(a); while uniform layers could be obtained by rotating the substrate uniformly during film growth. Besides, except the HfO_2 layer, other layers were flat. We used the average thickness (t_{HfO_2}) to denote the thickness of the wedge-shaped HfO_2, which varied from 3 nm to 33 nm. Four-probe electrical measurements revealed that the resistance of the HfO_2 layer is approximately on the order of MΩ. Furthermore, the deposition of HfO_2 did not reduce the resistance or the Hall resistance (R_H) of the Co/Pt layer, indicating that the HfO_2 layer is well insulated and the shunt effect from HfO_2 is negligible. The in-plane magnetic hysteresis (M–H) loop and out-of-plane M–H loop for the sample with $t_{HfO_2} = 25$ nm are shown in Fig. 1(b). The results reveal that the in-plane saturation field and out-of-plane saturation field are 1000 Oe (1 Oe = 79.5775 A·m^{-1}) and 140 Oe, respectively. The square out-of-plane M–H loop indicates strong perpendicular magnetic anisotropy of the film. The values of saturation magnetization (M_s) were measured in samples with varying HfO_2 thickness. The results show that M_s is approximately 800 emu/cm^3 and M_s is essentially unchanged with a thickness of t_{HfO_2}. For electrical characterization, the films were patterned into Hall-bar structures, each with 20 μm in length and 5 μm in width, by using lithography and ion milling. The Hall resistance measurements (with a sensor current of 0.1 mA) for the samples with t_{HfO_2} ranging from 3 nm to 33 nm are shown in Fig. 1(c). The results indicate that the field-induced change in the Hall resistance (ΔR_H) is about 1.23 Ω, which does not vary with HfO_2 thickness.

Figure 1(d) shows the effective perpendicular anisotropy field (H_K) as a function of HfO_2 thickness, where we used films with uniform HfO_2 thickness (not wedge-shaped) for the characterization of H_K (characterized by the electrical measurement and is explained in the supplementary materials S1). The result shows that H_K of the Pt/Co layer is significantly influenced by the HfO_2 buffer layer, with an observable decrease at 25 nm. The decrease in H_K may originate from the phase transition in the HfO_2 film. It is established that HfO_2 has three different structures: tetragonal, orthorhombic, and monoclinic phases. These different phases have preferences with respect to the film thickness. The orthorhombic phase, which is responsible for the ferroelectricity in this material, decreases when the thickness of HfO_2 exceeds a certain value,[25,26] while the nonpolarized monoclinic phases prefer larger thicknesses. The critical thickness for such a phase transition is approximately 30 nm, at which the ferroelectricity of HfO_2 normally quickly decreases.[25,27] The critical thickness for the phase transition aligns with the thickness for the drop H_K.

This can be understood as follows: first, the structural evolution (the film could change from orthorhombic phase to monoclinic phase) during the phase transition results in a change in lattice strain for the film deposited on it, consequently changing the magnetic properties of the Pt/Co layer due to magnetoelectric effects. Second, the decrease in ferroelectricity during the phase transition also influences the magnetic properties of Pt/Co due to the coupling between magnetism and ferroelectricity.[28]

It should be noted that although the insertion of a 3-nm-thick Pt layer between HfO_2 and Co could reduce the coupling strength, it could not eliminate the coupling. This is because 3-nm-thick Pt can also be treated as a magnetic film, as Pt can be easily magnetized by the Co film due to the magnetic proximity effect. However, the exact physical origin still needs further confirming.

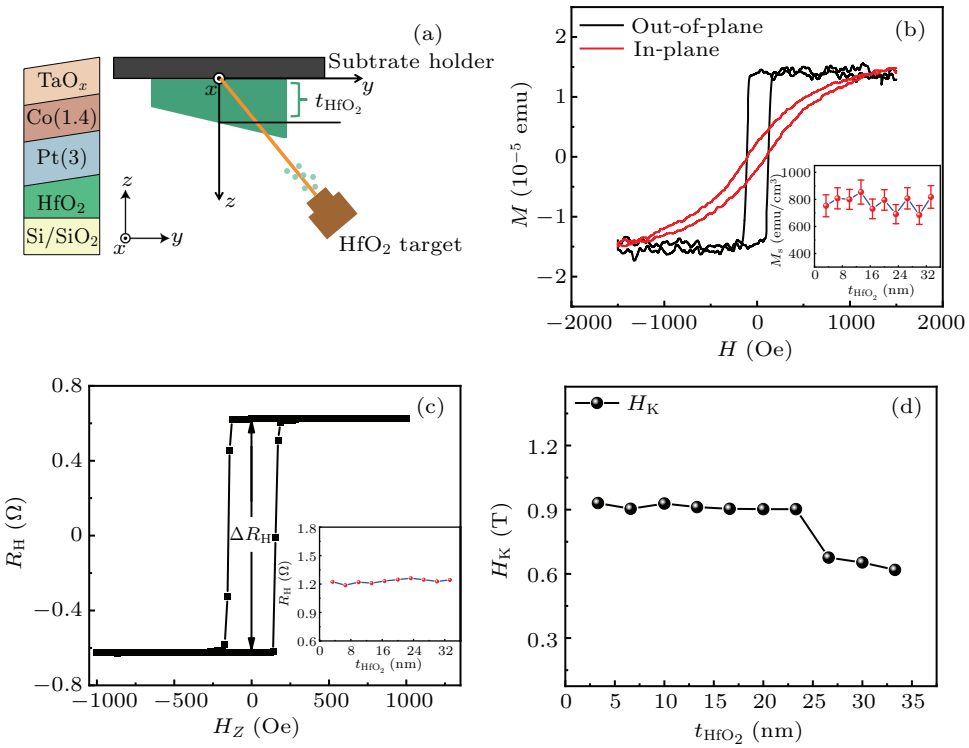


Fig. 1. (a) Schematic diagram of the film stacks (left), with wedge-shaped HfO_2 realized by using the oblique angle sputtering technique (right). (b) In-plane and out-of-plane magnetic hysteresis loop for the film with $t_{HfO_2} = 25$ nm, with inset showing M_s as a function of the HfO_2 thickness. (c) Out-of-plane R_{AHE} loop for the film with $t_{HfO_2} = 25$ nm, with inset displaying R_H with various HfO_2 thicknesses. (d) H_K as a function of HfO_2 thickness, with films with uniform HfO_2 thickness (not wedge-shaped) used for characterizing H_K.

3. SOT switching

Next, the SOT switching of the sample was characterized. Figure 2(a) shows the setup for the experiment. To drive the SOT switching of the magnetization, successive current pulses with a duration of 30 μs (current from negative value to positive value and then back to negative value) were applied along the x axis of the Hall bar, while a small sensing current of 0.1 mA was applied after each pulse to detect the magnetization state via R_H ($R_H \propto M_z$). External fields of different amplitudevalues of H_x along the current direction were applied to assist the switching. Figure 2(b) shows the switching behavior for the film with $t_{HfO_2} = 25$ nm. The R_H loops can be observed clearly when current pulses of various amplitudes are scanned, except for the case with $H_x = 10$ Oe. Notably, switching occurs even in the absence of H_x, demonstrating that the field-free switching is realized in these devices. In control experiments, it was found that the field-free switching does not occur in device with a flat HfO_2 buffer layer or in device without an HfO_2 buffer layer, underscoring that the wedge-shaped HfO_2 plays a critical role in realizing the field-free switching. The switching does not occur when $H_x = 10$ Oe, and the switching polarity reverses across $H_x = 10$ Oe. The reversal of switching polarity is consistent with the typical characteristic of SOT switching of perpendicular magnetization, indicating the SOT origin of the switching. the reversal of the switching polarity at $H_x = 10$ Oe also indicates that wedge-HfO_2 can induce a 10-Oe effective field, which promotes switching at zero field. Figure 2(c) shows the current ($H_x = 0$ Oe) and field induced change of Hall resistance (ΔR_H). The results show that the current-induced switching ΔR_H is 1.1 Ω, which is nearly 90% of the field-induced change of R_H (R_H^{max}), which means that the field-free switching ratio (defined as $\Delta R_H/R_H^{max} \times 100\%$) is 90%. This value is comparable to that achieved by using wedge-shaped ferromagnet.[29] To quantitatively evaluate the field-free switching for samples with t_{HfO_2}, figure 2(d) shows the H_x-dependent switching ratio, for samples with different values of t_{HfO_2}. These results reveal that the switching ratio increases with the amplitude of H_x and saturates when H_x reaches 100 Oe. The zero switching ratio occurs when $H_x = 10$ Oe, indicating that the wedge-shaped HfO_2 can generate an effective field of approximately 10 Oe. To assess device endurance, magnetization was alternately switched by using positive and negative current pulses (±13 mA), as shown in Fig. 2(e). After approximately 560 switching cycles, the Hall resistances in two distinct states do not show observable decay, indicating that our system has high durability. In a device with either a uniform HfO_2 buffer layer or no HfO_2 layer, field-free switching was not achievable, highlighting that the wedge-shaped HfO_2 buffer plays a pivotal role in facilitating

field-free switching. Figure 2(d) also reveals that for samples with different values of t_{HfO_2}, the field-free switching ratio (at $H_x = 0$) exhibits an observable difference. Figure 2(f) shows the field-free switching ratio as a function of t_{HfO_2}. The results reveal that with the increase of t_{HfO_2}, the switching ratio first increases and then decreases with an optimized switching ratio observed at $t_{HfO_2} = 25$ nm, at which the switching ratio could reach 90%.

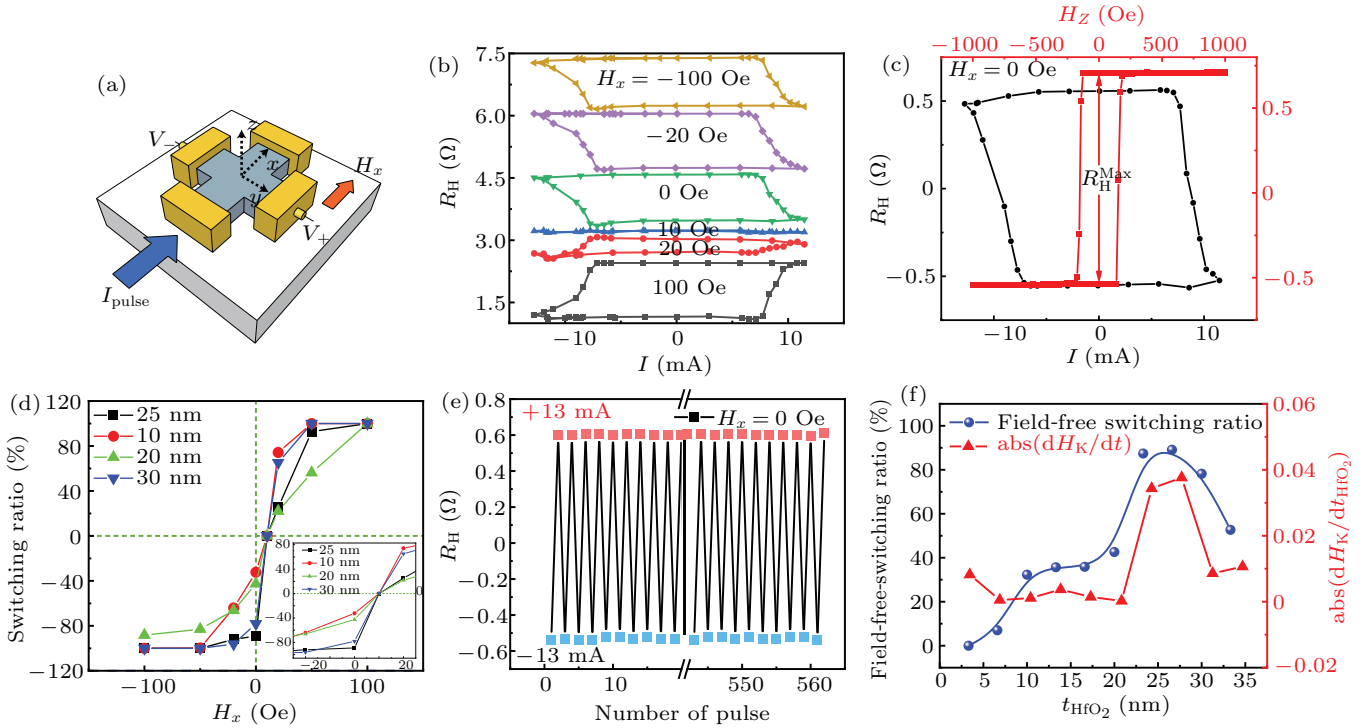


Fig. 2. (a) Schematic diagram of experimental setup. (b) SOT switching for sample with $t_{HfO_2} = 25$ nm, measured at different values of H_x. (c) Comparison of the field and current induced ($H_x = 0$) change of the R_H. (d) Switching ratios as a function of H_x for samples with different values of t_{HfO_2}. (e) Switching stability for the sample with $t_{HfO_2} = 25$ nm. Negative (−13 mA) current pulse and positive (+13 mA) current pulse are alternatively applied; R_H does not decay after approximately 500 switching cycles. (f) Blue dot line represents the field-free switching ratio for samples with different values of t_{HfO_2}. Red line corresponds to the absolute value of the first derivative of H_K with respect to t_{HfO_2}, calculated from Fig. 1(d).

The physical origin of the field-free switching is then discussed. It is important to note that the switching mechanism differs from that in the MgO buffer layer.[21] Previous studies have indicated that MgO buffer layers can also lead to field-free switching, which is attributed to the out-of-plane spin current induced by spin reflection. However, there are two reasons for a different mechanism in this study. First, the experiment demonstrates that only wedge-shaped HfO_2 buffer layer leads to field-free switching, unlike uniform HfO_2 layer. This contradicts the mechanism of out-of-plane polarized spin current-induced field-free switching, which does not depend on symmetry breaking. The absence of a loop shift at zero external in-plane bias field, as seen in supplementary materials, further indicates the noninvolvement of an out-of-plane polarized spin current. Additionally, the saturation thickness of the switching ratio is 25 nm, inconsistent with the spin tunneling length of HfO_2, which is typically below 10 nm. This inconsistency excludes the possibility of spin reflection-induced out-of-plane spin current-induced field-free switching. The field-free switching is not induced either by uneven current density due to shunting effects,[30] as experiments demonstrate high resistance in HfO_2 and negligible influence on Hall resistance. We attribute the field-free switching in the system to the anisotropy gradient induced by the wedged-shaped HfO_2 buffer layer. As shown in Fig. 1(d), the H_K of Co changes with the thickness of the HfO_2 buffer layer (t_{HfO_2}). For the presented wedge-shaped HfO_2, the thickness gradient along the wedge structure (y direction) can result in a nonuniform H_K in the film structure, and such a lateral anisotropy gradient (dH_K/dy) could induce field-free switching.[24,29,31] Our micromagnetic simulation further demonstrated that the field-free switching can be realized in the system with a lateral H_K gradient but cannot when H_K is uniform (see the supplementary materials). Figure 1(d) shows that at 25 nm, H_K decreases and attains a maximum value of the H_K gradient (dH_K/dt_{HfO_2}). This means that when $t_{HfO_2} = 25$ nm, H_K is most sensitive to the thickness variation, thus the dH_K/dy along the wedge should have a maximum value if the slope of the wedge is assumed to be fixed (dt_{HfO_2}/dy, mainly determined by the angle between the substrate and the sputtering target, which is fixed in this study). The t_{HfO_2}, dependent on dH_K/dt_{HfO_2}, could further be obtained from the first deriva-

tive of Fig. 1(d), and is plotted in Fig. 2(d). The magnitude of the t_{HfO_2}, dependent on dH_K/dt_{HfO_2}, is consistent with the field-free switching ratio, both of which have maximum values when $t_{HfO_2} \approx 25$ nm, demonstrating that the H_K gradient plays a critical role in establishing field-free switching. The lateral H_K gradient-induced field-free switching is understood by analyzing the mirror symmetry as discussed above, the field-free switching only occurs when mirror symmetry is broken. The lateral H_K gradient (perpendicular to the current direction) could break the mirror symmetry and facilitate field-free switching, which is similar to that in Ta/CoFeB/MgO systems with wedge-shaped MgO capping layer.[29,30]

4. Second harmonic measurement

The current-induced SOT field was quantitatively evaluated by analyzing the harmonic Hall voltage. As indicated in the inset of Fig. 3(a), we measured the first harmonic Hall voltage (V_ω) and the second harmonic Hall voltage ($V_{2\omega}$) under an alternating current (I_{ac}) ($\omega = 13.7$ Hz) along the x direction, while sweeping a large enough in-plane external magnetic field along the current direction.

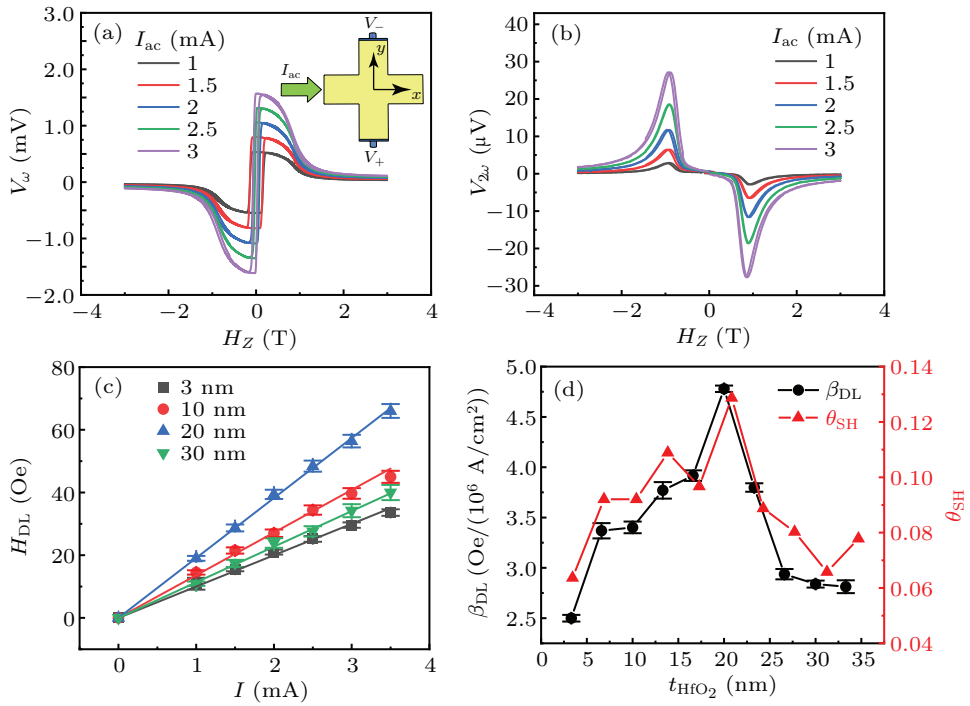


Fig. 3. (a)–(b) The first and second harmonic Hall voltages as a function of in-plane magnetic field H_x under different amplitudes of I_{ac} with $t_{HfO_2} = 3$ nm, with inset showing experiment setup schematically. (c) H_{DL} as a function of I_{ac}, for films with different values of t_{HfO_2}. (d) β_{DL} and θ_{SH} as a function of t_{HfO_2}.

Figures 3(a) and 3(b) show the field dependence of V_ω, $V_{2\omega}$ for films with $t_{HfO_2} = 3$ nm, which are measured under different values of I_{ac}. The in-plane damping-like SOT effective field (H_{DL}) could be estimated by fitting high-field data through the following equation:

$$R_{xy}^{2\omega} = \frac{\Delta R_H^{max}}{2} \frac{H_{DL}}{|H_x| - H_k} + R_{offset}, \tag{1}$$

where R_{offset} is the resistance offset. We characterize the H_{DL} for samples with different values of t_{HfO_2} as shown in Fig. 3(c). For all the samples, the values of H_{DL} exhibit a linear dependence with the amplitude of I_{ac}, demonstrating the current origin of the H_{DL}. The values of H_{DL} have distinguishable differences for the samples with different values of t_{HfO_2}. To quantify this difference, we further calculate the in-plane spin torque efficiency, which is defined as $\beta_{DL} = H_{DL}/J$, where J is the current density. The spin Hall angle of the device could further be calculated from the following equation:

$$\theta_{SH} = \left(\frac{2e}{\hbar}\right) \mu_0 M_s t_{FM} \beta_{DL}, \tag{2}$$

where e, $\hbar$, and μ_0 are the elementary charge, reduced Planck constant, and permeability of vacuum, respectively; M_s and t_{FM} are the saturation magnetization and thickness of the FM, respectively. We plot the and θ_{SH} as a function of t_{HfO_2} as shown in Fig. 3(d). With the increase of t_{HfO_2}, both β_{DL} and θ_{SH} first increase and reach their maximum values when the thickness of HfO_2 increases to 20 nm, after that β_{DL} decreases with the increase of t_{HfO_2}. β_{DL} and θ_{SH} each exhibit a peak value at 20 nm. This behavior is different from that of the field-free switching,whose maximum is at 25 nm. Such a discrepancy can be attributed to pinning effects. The SOT effective

field is not the only factor affecting the switching current. Additionally, the pinning field significantly affects the switching current as discussed by Zhu *et al.*[31] In our samples, due to defects and inevitable roughness at the Hall bar structure's edge, the pinning effects could be considerable, as evidenced by the larger H_c in the out-of-plane Hall loop (device) than that in the VSM (film). The pinning field varies across devices,resulting in the discrepancy between the switching current and the SOT effective field.

5. Conclusions

In conclusion, field-free switching has been demonstrated in a wedge-shaped HfO_2/Pt/Co/TaO_x structure. The field-free switching ratio and spin–orbit efficiency exhibit the thickness dependence of HfO_2, peaking at 25 nm. This approach differs from previously reported wedge-shaped capping layer-induced field-free switching strategies,[18–20] as HfO_2 does not contact the FM layer. This is attributed to the asymmetric magnetic anisotropy of Co induced by the wedge-shaped HfO_2 buffer layer. It is shown that the perpendicular magnetic anisotropy of Co displays a thickness dependence of HfO_2, with a maximum gradient at 25 nm, correlating with the field-free switching ratio and SOT efficiency. These results demonstrate that field-free switching can be achieved by designing buffer layer, thus presenting a new method of designing spin–orbit devices.

Acknowledgements

Project supported by the National Natural Science Foundation of China (Grant No. 12274108), the Natural Science Foundation of Zhejiang Province, China (Grant Nos. LY23A040008 and LY23A040008), and the Basic Scientific Research Project of Wenzhou, China (Grant No. G20220025).

References

[1] Shao Q M, Li P, Liu L Q, Yang H, Fukami S, Razavi A, Wu H, Wang K, Freimuth F, Mokrousov Y, Stiles M D, Emori S, Hoffmann A, Åkerman J, Roy K, Wang J P, Yang S H, Garello K and Zhang W 2021 *IEEE T. Magn.* **57** 1

[2] Manchon A, Zelezny J, Miron I M, Jungwirth T, Sinova J, Thiaville A, Garello K and Gambardella P 2019 *Rev. Mod. Phys.* **91** 35004

[3] Ramaswamy R, Lee J M, Cai K M and Yang H 2018 *Appl. Phys. Rev.* **5** 31107

[4] Aradhya S V, Rowlands G E, Oh J, Ralph D C and Buhrman R A 2016 *Nano Lett.* **16** 5987

[5] Garello K, Avci C O, Miron I M, Baumgartner M, Ghosh A, Auffret S, Boulle O, Gaudin G and Gambardella P 2014 *Appl. Phys. Lett.* **105** 212402

[6] Fukami S, Anekawa T, Zhang C and Ohno H 2016 *Nat. Nanotechnol.* **11** 621

[7] Miron I M, Garello K, Gaudin G, Zermatten P J, Costache M V, Auffret S, Bandiera S, Rodmacq B, Schuhl A and Gambardella P 2011 *Nature* **476** 189

[8] Liu L Q, Pai C F, Li Y, Tseng H W, Ralph D C and Buhrman R A 2012 *Science* **336** 555

[9] Baek S H C, Amin V P, Oh Y W, Go G, Lee S J, Lee G H, Kim K J, Stiles M D, Park B G and Lee K J 2018 *Nat. Mater.* **17** 509

[10] Fukami S, Zhang C L, DuttaGupta S, Kurenkov A and Ohno H 2016 *Nat. Mater.* **15** 535

[11] Kong W J, Wan C H, Wang X, Tao B S, Huang L, Fang C, Guo C Y, Guang Y, Irfan M and Han X F 2019 *Nat. Commun.* **10** 233

[12] Lau Y C, Betto D, Rode K, Coey J M D and Stamenov P 2016 *Nat. Nanotechnol.* **11** 758

[13] Zhao Z Y, Smith A K, Jamali M and Wang J P 2020 *Adv. Electron. Mater.* **6** 1901368

[14] Hu S, Shao D F, Yang H L, Pan C, Fu Z X, Tang M, Yang Y M, Fan W J, Zhou S M, Tsymbal E Y and Qiu X P 2022 *Nat. Commun.* **13** 4447

[15] MacNeill D, Stiehl G M, Guimaraes M H D, Buhrman R A, Park J and Ralph D C 2017 *Nat. Phys.* **13** 300

[16] Safeer C K, Jué E, Lopez A, Buda-Prejbeanu L, Auffret S, Pizzini S, Boulle O, Miron I M and Gaudin G 2016 *Nat. Nanotechnol.* **11** 143

[17] Wu H, Nance J, Razavi S A, Lujan D, Dai B Q, Liu Y X, He H R, Cui B S, Wu D, Wong K, Sobotkiewich K, Li X Q, Carman G P and Wang K L 2021 *Nano Lett.* **21** 515

[18] Chen R Y, Cui Q R, Liao L Y, Zhu Y M, Zhang R Q, Bai H, Zhou Y J, Xing G Z, Pan F, Yang H X and Song C 2021 *Nat. Commun.* **12** 3113

[19] Yu G Q, Upadhyaya P, Fan Y B, Alzate J G, Jiang W J, Wong K L, Takei S, Bender S A, Chang L T, Jiang Y, Lang M R, Tang J S, Wang Y, Tserkovnyak Y, Amiri P K and Wang K L 2014 *Nat. Nanotechnol.* **9** 548

[20] Razavi A, Wu H, Shao Q M, Fang C, Dai B Q, Wong K, Han X F, Yu G Q and Wang K L 2020 *Nano Lett.* **20** 3703

[21] Jin T L, Lim G J, Poh H Y, Wu S, Tan F N and Lew W S 2022 *ACS Appl. Mater. Interfaces* **14** 9781

[22] Schroeder U, Park M H, Mikolajick T and Hwang C S 2022 *Nat. Rev. Mater.* **7** 653

[23] Peng W L, Zhang J Y, Feng G N, Xu X L, Yang C, Jia Y L and Yu G H 2019 *Appl. Phys. Lett.* **115** 172403

[24] Wu H, Nance J, Razavi S A, Lujan D, Dai B Q, Liu Y X, He H R, Cui B S, Wu D, Wong K, Sobotkiewich K, Li X Q, Carman G P and Wang K L 2021 *Nano Lett.* **21** 515

[25] Park M H, Kim H J, Kim Y J, Lee W, Moon T and Hwang C S 2013 *Appl. Phys. Lett.* **102** 242905

[26] Hoffmann M, Schroeder U, Schenk T, Shimizu T, Funakubo H, Sakata O, Pohl D, Drescher M, Adelmann C, Materlik R, Kersch A and Mikolajick T 2015 *J. Appl. Phys.* **118** 72006

[27] Quan Z Y, Wang M M, Zhang X, Liu H H, Zhang W and Xu X H 2020 *AIP Adv.* **10** 85024

[28] Chu Y H, Martin L W, Holcomb M B, Gajek M, Han S J, He Q, Balke N, Yang C H, Lee D, Hu W, Zhan Q, Yang P L, Fraile-Rodríguez A, Scholl A, Wang S X and Ramesh R 2008 *Nat. Mater.* **7** 478

[29] Yu G Q, Upadhyaya P, Fan Y B, Alzate J G, Jiang W J, Wong K L, Takei S, Bender S A, Chang L T, Jiang Y, Lang M R, Tang J S, Wang Y, Tserkovnyak Y, Amiri P K and Wang K L 2014 *Nat. Nanotechnol.* **9** 548

[30] Wu H, Zhang J, Cui B, Razavi S A, Che X, Pan Q, Wu D, Yu G, Han X and Wang K L 2022 *Materials Futures* **1** 22201

[31] Zhu L J, Ralph D C and Buhrman R A 2021 *Phys. Rev. Appl.* **15** 24059